

Temporal and Spatial Variations in Electron Density and Blackbody Temperature in the Initial Phase of a Laser Ablation BN Plasma

Koichi SASAKI, Shin YASUDA¹⁾ and Noriharu TAKADA¹⁾

*Plasma Nanotechnology Research Center, Nagoya University,
Furo-cho, Chikusa-ku, Nagoya 464-8603, Japan*

¹⁾*Department of Electrical Engineering and Computer Science, Nagoya University,
Furo-cho, Chikusa-ku, Nagoya 464-8603, Japan*

(Received 25 February 2008 / Accepted 27 March 2008)

Optical emission spectroscopy was used for examining the temporal variations in the spatial distributions of the blackbody temperature and electron density of plasmas produced by laser ablation of a BN target in ambient nitrogen gas. The blackbody temperature was estimated by fitting the continuum component in the optical emission spectrum using the Planck's law of radiation, and the electron density was evaluated from the Stark broadening of a line emission of a B atom. The blackbody temperature was evaluated to be close to 10^4 K and the electron density was on the order of 10^{17} - 10^{18} cm^{-3} , immediately after the irradiation of the laser pulse on the target. The dynamics of the blackbody temperature and the electron density were understood by considering plasma expansion and the confinement effect of ambient gas.

© 2008 The Japan Society of Plasma Science and Nuclear Fusion Research

Keywords: electron density, blackbody temperature, spatiotemporal variation, optical emission spectroscopy, laser ablation plasma

DOI: 10.1585/pfr.3.023

1. Introduction

Remarkable features of a laser ablation plasma in comparison with a discharge plasma are the high density, the high temperature, and the high pressure particularly in the initial phase after the irradiation of a laser pulse onto a solid-state target. These features should have positive effects in the synthesis of crystalline nanoparticles. Therefore, it is important to evaluate the density and temperature of a laser ablation plasma, and understand their effects on material syntheses. Since laser-ablation plasma has a fast temporal variation and a dynamic spatial distribution, any diagnostic methods applicable to laser ablation plasma should have fine temporal and spatial resolutions. To date, optical emission spectroscopy is exclusively applied to measure electron densities, electron temperatures, and blackbody temperatures of laser-ablation plasmas [1–5].

Recently, Komatsu and coworkers succeeded in synthesizing sp^3 -bonded BN of the 5H polytypic form by laser ablation of a BN target in an ambient NH_3 plasma [6, 7]. This sp^3 -bonded 5H-BN is a new material, and is a semiconductor with a wide band gap corresponding to photoluminescence at a wavelength of 225 nm [6]. This material can yield strong electron field emission [7]. Although the synthesis mechanism of 5H-BN is not yet understood, it is speculated that the high-temperature, high-pressure plasma

produced by laser ablation of a BN target is responsible for the growth of the high-pressure phase sp^3 -bonded crystal structure. In this study, we examine the blackbody temperature and electron density of a laser-ablation BN plasma by optical emission spectroscopy. For understanding the dynamics of laser-ablation plasma in the initial phase, we conducted measurements with temporal and spatial resolutions.

2. Experiment

We used the experimental apparatus shown in Fig. 1. A stainless-steel vacuum chamber was evacuated below 3×10^{-6} Torr using a turbomolecular pump. After evacuation, pure N_2 gas was introduced at a flow rate of 100 sccm from the bottom of the chamber. The gas pressure was controlled from 0 to 10 Torr by changing the evacuation rate using a variable conductance valve. A sintered BN target was installed on a rotating holder in the vacuum chamber. YAG laser pulses at a wavelength of 266 nm irradiated the BN target from the normal direction. The energy, repetition rate, and duration of the YAG laser pulses were 37 mJ, 10 Hz, and 8 ns, respectively. The YAG laser beam was focused using a lens, and the fluence on the target surface was estimated to be 3 J/cm^2 .

Another lens was used to project the optical emission in front of the target onto an optical fiber array. The optical fiber array consisted of 20 linearly-aligned cores, and

author's e-mail: sasaki@nuee.nagoya-u.ac.jp

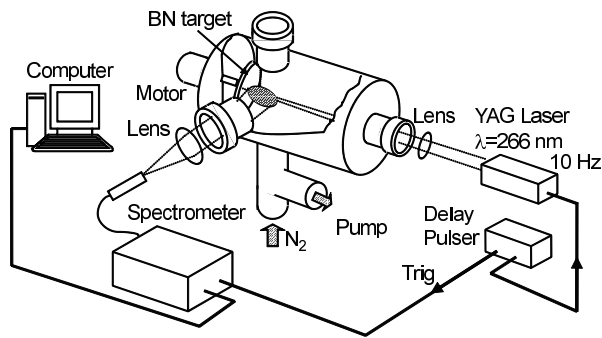


Fig. 1 Experimental apparatus.

was positioned to observe the axial distribution of the optical emission. The other end of the optical fiber array was placed close to the entrance slit of the monochromator with a focal length of 500 mm. We used gratings with 600 and 2400 grooves/mm, that corresponded to wavelengths resolutions of 0.2 and 0.05 nm, respectively. The exit side of the monochromator was connected to a charge-coupled device camera with a gated image intensifier (ICCD camera), which recorded optical emission spectra at various distances from the target surface. The gate width was 10 ns. The wavelength dependence of the sensitivity of the monochromator including the ICCD camera was calibrated using a standard tungsten lamp. The spatial resolution corresponding to each core of the optical fiber array was 0.25 mm. The temporal variations in the optical emission spectra were obtained by changing the delay time between the irradiation of the YAG laser pulse and the trigger to the gate of the ICCD camera. We accumulated spectra from 50 laser shots to improve the signal-to-noise ratio and compensate for poor shot-to-shot reproducibility.

3. Results and Discussion

3.1 Optical emission spectrum and data analysis

A typical optical emission spectrum in the range from 300 to 800 nm is shown in Fig. 2 (a). This spectrum was obtained without the injection of N_2 gas (0 Torr), 50 ns after the irradiation of the YAG laser pulse. The grating with 600 grooves/mm was used. The measurement position was 1 mm from the target. The optical emission spectrum was composed of several line emissions, which were assigned as BII (345.13 nm, the $1P_1^0-1D_2$ transition), BI (249.68 and 249.77 nm, the $2P_{1/2}^0-2S_{1/2}$ and $2P_{3/2}^0-2S_{1/2}$ transitions), and NI (742.36, 744.23, and 746.83 nm, the $4P_{1/2}^0-4S_{3/2}^0$, $4P_{3/2}^0-4S_{3/2}^0$ and $4P_{5/2}^0-4S_{3/2}^0$ transitions). The line emission at around 582 nm may be due to an impurity, and its most probable assignments are CI and CII. Second-order diffraction of the YAG laser light was also detected.

As shown in Fig. 2 (a), the spectrum contained a broad continuum component. This continuum emission was believed to be due to blackbody radiation. Under the assump-

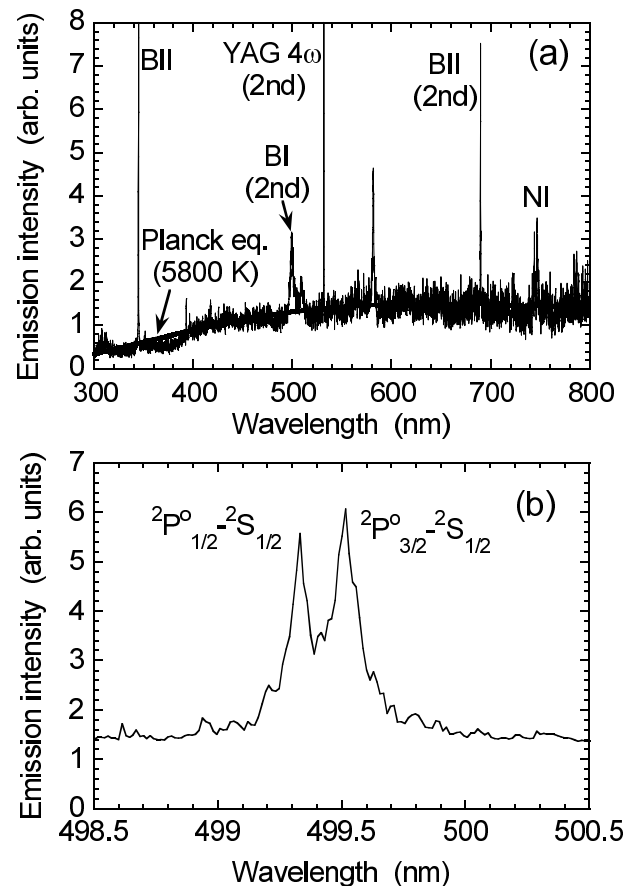


Fig. 2 Optical emission spectra observed in vacuum, 50 ns after irradiation of the YAG laser pulse. The measurement position was 1 mm from the target surface. (a) The wide-range spectrum observed using a grating with 600 grooves/mm. The thick solid curve represents the Planck's law of radiation corresponding to a blackbody temperature of 5800 K. (b) The fine-resolution spectrum of the BI ($2P^0-2S$) line observed using a grating with 2400 grooves/mm.

tion of the blackbody radiation, the continuum component is approximated using the Planck's law of radiation. The thick solid curve shown in Fig. 2 (a) represents the Planck's law of radiation corresponding to a blackbody temperature of 5800 K. The continuum component was well approximated using the Planck's law of radiation. Thus, we evaluated the blackbody temperature of the plasma by optical emission spectroscopy.

Figure 2 (b) shows a fine-resolution spectrum of the BI ($2P^0-2S$) line observed using a grating with 2400 grooves/mm. This line is composed of two fine-structure components. Although the fine-structure components overlapped partially, the widths of the two peaks were broader than the wavelength resolution of the spectrometer. Since Doppler broadening is expected to be narrower than the wavelength resolution, the additional width is understood to be due to Stark broadening. The Stark broadening width (FWHM) $\Delta\lambda_{1/2}$ is a function of the elec-

tron density n_e (in cm^{-3}), which includes the electron impact width parameter W and the ion broadening parameter A [3], and is given by

$$\Delta\lambda_{1/2} = 2W\left(\frac{n_e}{10^{16}}\right) + 3.5A\left(\frac{n_e}{10^{16}}\right)\left[1 - \frac{3}{4}N_D^{-1/3}\right]W\left(\frac{n_e}{10^{16}}\right), \quad (1)$$

where N_D is the number of particles in the Debye sphere. Although the overlapping of the two fine-structure components was problematic, we considered that the analysis of the BI ($^2\text{P}^{\circ}\text{-}^2\text{S}$) line was the best choice for evaluating the electron density in the line emissions shown in Fig. 2 (a). The spectrum shown in Fig. 2 (b) was separated into two fine-structure components having the same width using a curve-fitting software. The instrumental broadening was deconvoluted for evaluating the Stark broadening width. The electron impact width parameter and the ion broadening parameter of the BI ($^2\text{P}^{\circ}\text{-}^2\text{S}$) line are listed in the literature [8–10]. We assumed an electron temperature of 10 eV for estimating the electron density, since we did not evaluate the electron temperature from the optical emission spectrum. The assumption of 10 eV is based on a report on the electron temperature of a laser ablation plasma [11]. If we assume an electron temperature of 1 eV, the electron density becomes roughly three times that evaluated at 10 eV. We thus evaluated the electron density of the plasma by optical emission spectroscopy.

3.2 Blackbody temperature

Figure 3 shows the temporal variation in the spatial distribution in the blackbody temperature. This result was obtained by repeating the data analysis at various measurement positions and delay times, after the irradiation of the YAG laser pulse. The error bars illustrated in Fig. 3 represent the ambiguity in the fitting between the spectral distribution of the continuum component and the Planck's law of radiation. As shown in Fig. 3, the blackbody temperatures at delays within 100 ns were approximately 5000–10000 K. The evaluation of the blackbody temperature was difficult after 100 ns because of the low amplitude of the continuum component in the optical emission spectra.

When nitrogen gas was not injected (0 Torr), as shown in Fig. 3 (a), the spatial distribution of the blackbody temperature 20 ns after irradiating the YAG laser pulse had a peak at a distance of approximately 1.4 mm from the target surface. The spatial distribution was rather confined even in the initial phase (20 and 50 ns). In contrast, at gas pressures of 2 and 10 Torr, the blackbody temperature had steep distributions, as shown in Figs. 3 (b) and 3(c). The peak positions were 0.8 and 0.4 mm from the target at gas pressures of 2 and 10 Torr, respectively. In other words, the peak position was closer to the target at a higher gas pressure. In addition, as shown in Fig. 3, the temporal decrease in the blackbody temperature at the peak position was slower at a higher gas pressure, whereas at a long dis-

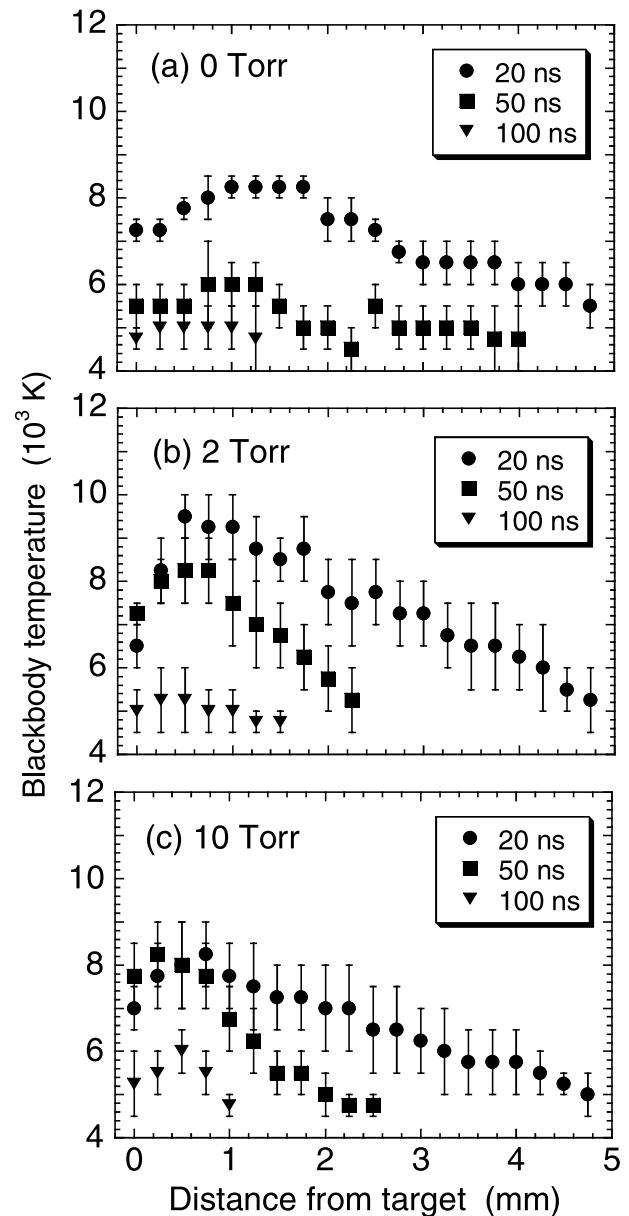


Fig. 3 Temporal variation in the spatial distribution of the blackbody temperature observed at gas pressures of (a) 0 Torr, (b) 2 Torr, and (c) 10 Torr.

tance from the target, the decrease in the blackbody temperature was roughly independent of gas pressure.

3.3 Electron density

The temporal variation in the spatial distribution of the electron density is shown in Fig. 4. In this analysis, we summed up spectra obtained by three cores of the optical fiber array to improve the signal-to-noise ratio. The horizontal error bars shown in Fig. 4 indicate the range of the data summation. The vertical error bars result from ambiguity in the evaluation of the Stark width. Evaluation of the electron density at delay times less than 50 ns was difficult, since the optical emission spectrum was gov-

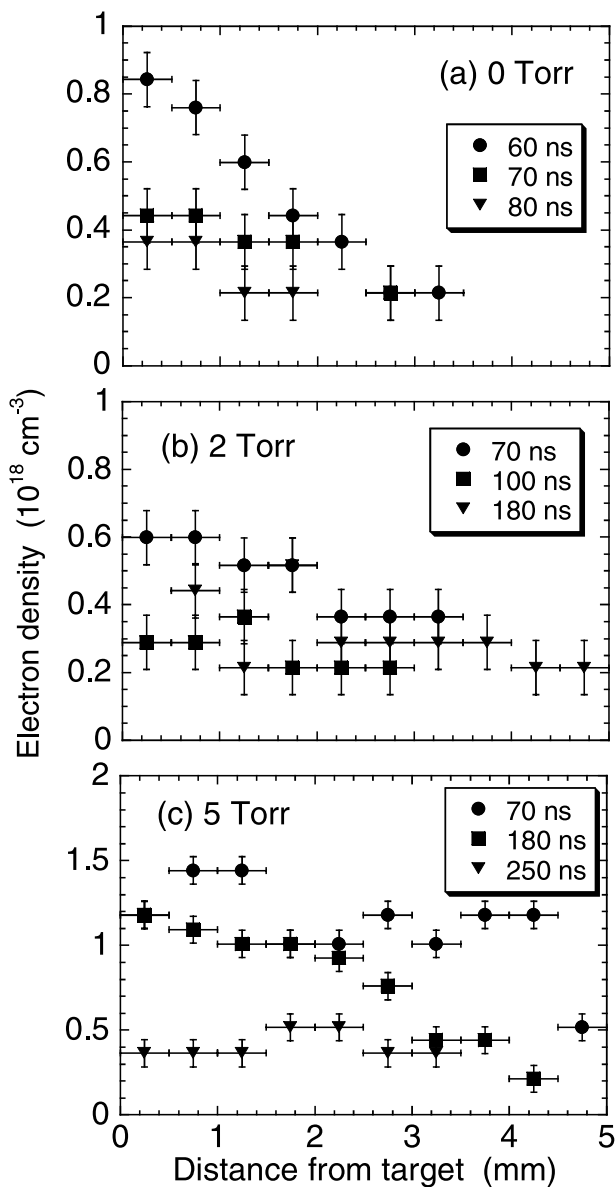


Fig. 4 Temporal variation in the spatial distribution of the electron density observed at gas pressures of (a) 0 Torr, (b) 2 Torr, and (c) 5 Torr.

erned by the continuum component. As shown in Fig. 4, we evaluated the electron density as being on the order of 10^{17} - 10^{18} cm^{-3} .

The electron density in the initial phase had a peak adjacent to the target surface and a steep decrease as the distance from the target increased. At long delay times (180 ns at 2 Torr, and 250 ns at 5 Torr), the spatial distribution of the electron density became uniform. The temporal decay of the electron density was much slower at higher gas pressures as shown in Fig. 4.

3.4 Discussion

Although the spectra including both line and continuum emissions, as shown in Fig. 2 (a), were observed at

delay times ranging from 50 to 100 ns, there is a possibility that the line and continuum components are emitted from different parts of the plasma. This is because the optical emission spectrum before 50 ns is governed by the continuum component, whereas only line emissions were observed in the optical emission spectrum after 100 ns. This result suggests that the continuum and line emissions are observed from dense and rarefied plasmas, respectively. Considering the radial distribution of the plasma density, the continuum component shown in Fig. 2 (a) may be emitted from the central part that has a high density, whereas the line emissions may be from the peripheral region that has a rarefied density. However, even if the continuum and line emissions do not represent the behavior of the entire region, it would be possible to present a brief discussion on the dynamics of the laser ablation plasma based on the results of optical emission spectroscopy.

The dynamics of the blackbody temperature and electron density are basically understood by considering the expansion of the plasma and the confinement effect of ambient gas. The blackbody temperature in ambient gas had a steeper distribution than in vacuum, which is attributed to the confinement of the plasma by ambient gas. The slower temporal decay of the blackbody temperature is also understood by assuming that adiabatic expansion is the dominant cooling mechanism of the plasma. Plasma expansion is restricted in ambient gas, resulting in the longer decay time constant of the blackbody temperature. Although collisions with ambient gas would contribute to a relatively rapid decrease in the blackbody temperature at a long distance from the target, the dominant cooling mechanism of the initial-phase laser-ablation plasma is considered to be adiabatic expansion.

Since a volume loss of electrons by recombination is not expected in the early-phase (< 250 ns) of a laser-ablation plasma [4], the temporal variation in the spatial distribution of the electron density shown in Fig. 4 is also understood by plasma expansion and confinement. The longer decay time constant of the electron density at a higher gas pressure is consistent with the confinement effect of ambient gas. The highest electron density at a gas pressure of 5 Torr, as shown in Fig. 4 (c), has not yet been understood; however additional ionization by collision of confined electrons would probably enhance the electron density.

4. Conclusions

We investigated blackbody temperatures and electron densities of laser-ablation BN plasmas by optical emission spectroscopy. Temporal and spatial variations in the blackbody temperature and electron density were examined using a linearly-aligned optical fiber array and a gated ICCD camera. The blackbody temperature 20 ns after irradiation of the YAG laser pulse was approximately 10^4 K. The electron density at 60-70 ns was on the order of 10^{17} -

10^{18} cm^{-3} . The temporal and spatial variations in the blackbody temperature and electron density are basically understood by considering plasma expansion and the confinement effect of ambient gas.

- [1] F.J. Gordillo-Vázquez, A. Perea, A.P. McKiernan and C.N. Afonso, *Appl. Phys. Lett.* **86**, 181501 (2005).
- [2] S.S. Harilal, B. O'Shay and M.S. Tillack, *J. Appl. Phys.* **98**, 013306 (2005).
- [3] N.M. Shaikh, B. Rashid, S. Hafeez, Y. Jamil and M.A. Baig, *J. Phys. D: Appl. Phys.* **39**, 1384 (2006).
- [4] S. Namba, R. Nozu, K. Takiyama and T. Oda, *J. Appl. Phys.* **99**, 073302 (2006).
- [5] S. Amoroso, R. Bruzzese, N. Spinelli, R. Velotta, M. Vitiello and X. Wang, *Appl. Phys. Lett.* **84**, 4502 (2004).
- [6] S. Komatsu, K. Kurashima, H. Kanda, K. Okada, M. Mitomo, Y. Moriyoshi, Y. Shimizu, M. Shiratani, T. Nakano and S. Samukara, *Appl. Phys. Lett.* **81**, 4547 (2002).
- [7] S. Komatsu, A. Okudo, D. Kazami, D. Golberg, Y.B. Li, Y. Moriyoshi, M. Shiratani and K. Okada, *J. Phys. Chem. B* **108**, 5182 (2004).
- [8] H.R. Griem, *Plasma Spectroscopy* (McGraw-Hill, New York, 1964).
- [9] H.R. Griem, *Principles of plasma spectroscopy* (Cambridge University Press, Cambridge, 1997).
- [10] H.R. Griem, *Spectral line broadening by plasmas* (Academic Press, New York, 1974).
- [11] B.Y. Man, Q.L. Dong, A.H. Wei, Q.G. Zhang, J.L. He and X.T. Wang, *J. Opt. A: Pure Appl. Opt.* **6**, 17 (2004).